

# Conditions for formation of germanium quantum dots in amorphous matrices by MeV ions: Comparison with standard thermal annealing

I. Bogdanović-Radović,<sup>\*</sup> M. Buljan, M. Karlušić, N. Skukan, I. Božičević, M. Jakšić, and N. Radić  
*Rudjer Bošković Institute, Bijenička cesta 54, 10000 Zagreb, Croatia*

G. Dražić  
*Jožef Stefan Institute, Jamova 39, 1000 Ljubljana, Slovenia*

S. Bernstorff  
*Sincrotrone Trieste, 34102 Basovizza, Italy*  
 (Received 21 August 2012; published 15 October 2012)

We investigate how MeV ions with different ion-beam parameters (ion type, electronic stopping power, and velocity) influence the formation, arrangement, and ordering quality in three types of (Ge + SiO<sub>2</sub>)/SiO<sub>2</sub> multilayer films. The multilayers differ in total thickness, Ge-rich layer thickness, and Ge content. The results show that the most important parameter for structural manipulation with MeV ions is the electronic stopping power  $S_e$ . Ion velocity is found to be another crucial parameter, while at the same time it can be seen that the multilayer type does not play an important role. The temperature increase within the ion tracks is estimated using the thermal spike model and cluster separation distribution. The structural changes produced by ion beams and estimated temperatures are compared to those obtained by standard thermal annealing. It is concluded that the estimated temperatures within the ion tracks are in excellent agreement with the annealing temperatures and with the structural changes observed in the irradiated multilayers. Furthermore, a characteristic parameter of the temperature profile that presents the model-predicted temperature increase is determined for which the structural changes caused by ion beams are comparable to those achieved by standard annealing.

DOI: [10.1103/PhysRevB.86.165316](https://doi.org/10.1103/PhysRevB.86.165316)

PACS number(s): 81.07.Ta, 68.65.Ac, 81.16.Dn, 61.46.Hk

## I. INTRODUCTION

Materials based on semiconductor quantum dots (QDs) are very interesting due to their size-tunable properties and many relevant applications.<sup>1</sup> The properties of such materials are highly influenced by the arrangement and size properties of the QDs and therefore it is important to achieve the controllable production of such materials. Especially interesting are materials based on semiconductor QDs, embedded in amorphous matrices. Ge QDs embedded in a SiO<sub>2</sub> matrix show strong quantum confinement effects,<sup>2</sup> nonlinear properties,<sup>3</sup> electroluminescence, and photoluminescence.<sup>4,5</sup>

Recently we have reported a method for the production of self-assembled QDs by ion-beam irradiation.<sup>6–8</sup> Self-assembly was induced by the passage of 3-MeV oxygen ions through (Ge + SiO<sub>2</sub>)/SiO<sub>2</sub> multilayer. The observed behavior was explained in terms of the electronic stopping values of the ions used for the irradiation and by the system efficiency for transfer of deposited energy into the thermal spike ( $g$ ). By electronic stopping, one means the slowing-down of ions due to inelastic collisions between bound electrons in the medium and the ion moving through it. Due to electron-phonon coupling, the ions cause a local temperature increase, which determines the diffusion rates of Ge atoms in the area around the ion trajectories. Thus, if the temperature is too low, there is no diffusion of Ge atoms and self-assembly cannot happen. On the contrary, the optimal temperature causes diffusion of Ge atoms and formation of Ge nuclei along the ion tracks. Based on this concept, we have developed a three-dimensional (3D) Monte Carlo model for the simulation of self-assembly by ion-beam irradiation.<sup>7,8</sup>

Herein we present and discuss the influence of different ion-beam properties such as ion type, energy, and stopping power values on the self-assembly process and structural changes in different (Ge + SiO<sub>2</sub>)/SiO<sub>2</sub> multilayer types. The effects produced by ion beams are compared to those produced by standard thermal annealing at different temperatures. The range of ion-beam parameters where the formation of Ge clusters and the Ge self-assembly process are optimal was explored. The influence of the ion velocity on the temperature increase was examined and found to be very important. The width parameter of the temperature profile within the ion tracks is determined by applying a recently developed method based on the thermal spike model and distribution of cluster separations.<sup>9</sup> This parameter is used for estimation of the temperature-increase profiles that are caused by the passage of various ion types through the investigated systems.

The results obtained show excellent agreement of the estimated temperatures within the ion tracks and structural changes in the multilayers. Finally, a characteristic parameter of the temperature profile was found for which the structural changes caused by ion beams are comparable to those achieved by standard annealing. The procedure presented may be applied to other similar systems for prediction of temperature changes caused by ion beams and for design of QD formation in them.

## II. EXPERIMENTAL

Multilayer films containing 20 (Ge + SiO<sub>2</sub>)/SiO<sub>2</sub> bilayers were deposited by magnetron sputtering on a Si(111) substrate

TABLE I. Description of three types of (Ge + SiO<sub>2</sub>)/SiO<sub>2</sub> multilayer films. Each multilayer contains 20 periods (bilayers) characterized by bilayer thickness ( $P$ ), Ge-rich-layer thickness ( $P_{\text{Ge}}$ ), and atomic percentages ( $c_{\text{Si,O,Ge}}$ ) of all elements in the Ge-rich layers.

Multilayer type	$P$ (nm)	$P_{\text{Ge}}$ (nm)	$c_{\text{Si}}$ (at%)	$c_{\text{O}}$ (at%)	$c_{\text{Ge}}$ (at%)
$S_1$	15	5	0.173	0.592	0.235
$S_2$	10.5	4.5	0.373	0.500	0.127
$S_3$	6	1.5	0.373	0.500	0.127

at room temperature (RT) under the working gas pressure of 0.7 Pa. All characteristics of three produced types of multilayer samples—total thicknesses ( $P$ ), Ge-rich-layer thicknesses ( $P_{\text{Ge}}$ ), and atomic percentages ( $c_{\text{Si,O,Ge}}$ )—are listed in Table I. After deposition, the multilayers were irradiated at RT ( $T_{\text{IRR}} = 300$  K) by various ions at one of the three ion fluences ( $D_1 = 5 \times 10^{14}$ ,  $D_2 = 1 \times 10^{15}$ , or  $D_3 = 2 \times 10^{15}$  ions/cm<sup>2</sup>) and one of the four ion-beam incidence angles with respect to the multilayer surface ( $\varphi_{\text{irr}} = 30, 45, 60,$  or  $90^\circ$ ). Ion beams used for irradiation together with their electronic stopping power values  $S_e$  for different layers are listed in Table II.

The internal structure of the material was investigated by the combination of grazing incidence small-angle x-ray scattering (GISAXS), scanning transmission electron microscopy (STEM) measurements, and Rutherford backscattering spectroscopy (RBS). GISAXS maps were measured at Synchrotron Elettra, Trieste, and at the SAXS beam line using a photon energy of 8 keV and a 2D image plate detector. Determination of the clustering of Ge atoms and the existence of a correlation in the cluster positions were analyzed by complementary GISAXS and TEM techniques. The GISAXS technique is especially suitable for the analysis of irradiation effects, because irradiation-induced structural changes in the films cause the appearance of strong correlation maxima (Bragg sheets) in their GISAXS maps. These sheets have a tilt angle dependent on the correlation of the structural features induced by irradiation.<sup>6-8,10-12</sup>

TABLE II. Ion beams used for irradiation together with their electronic stopping power values  $S_e$  in  $\alpha$ -SiO<sub>2</sub> and Ge + SiO<sub>2</sub> layers calculated using the SRIM 2008 code.<sup>16</sup>  $E$  denotes the energy of the ions used,  $\rho$  is the material density,  $c$  is the specific heat capacity,  $T(r = 0)$  is the temperature in the center of the track,  $T(r = a_0)$  is the maximal temperature at distance  $r = a_0$  from the center of the ion track, and  $g$  is the fraction of the energy deposited in the thermal spike.

Ion	$E$ (MeV)	$S_e$ (keV nm <sup>-1</sup> )	$\rho$ (g cm <sup>-3</sup> )	$c$ (J kg <sup>-1</sup> K <sup>-1</sup> )	$T(r = 0)$ (K)	$T(r = a_0)$ (K)	$g$
Ge + SiO <sub>2</sub> (12.7% Ge)							
<sup>16</sup> O	1	1.358	3.8	854	972	556	0.4
<sup>16</sup> O	3	2.303	3.8	854	1457	735	0.4
<sup>16</sup> O	15	2.330	3.8	854	873	520	0.2
<sup>28</sup> Si	6	3.920	3.8	854	2287	1040	0.4
<sup>28</sup> Si	15	4.896	3.8	854	2787	1224	0.4
Ge + SiO <sub>2</sub> (23.5% Ge)							
<sup>16</sup> O	1	1.469	4.7	777	945	546	0.4
<sup>16</sup> O	3	2.594	4.7	777	1458	735	0.4
<sup>16</sup> O	15	2.729	4.7	777	897	529	0.2
<sup>28</sup> Si	6	4.443	4.7	777	2301	1045	0.4
<sup>28</sup> Si	15	5.715	4.7	777	2881	1259	0.4

STEM measurements were performed using a JEOL 2010 F microscope, operated at 200 kV and equipped with a field-emission gun and a high-angle annular dark-field detector (HAADF) for Z-contrast imaging. RBS measurements were done using a 2-MeV He beam from the 6-MV tandem Van de Graaff accelerator at the Rudjer Bošković Institute, Zagreb. Backscattered spectra were collected using a particle detector placed at  $165^\circ$ .

### III. ION-BEAM-INDUCED FORMATION OF GERMANIUM NANOCLUSTERS

For all multilayer films the energy of the ions used was selected to be high enough to ensure approximately straight trajectories of ions through the multilayer with the end of the projected range located deep in the Si substrate. O ions (1 MeV) entering the target under  $\varphi_{\text{irr}} = 60^\circ$  stop at  $1.3 \mu\text{m}$  below the surface, and Si ions (15 MeV) stop at  $5.5 \mu\text{m}$ , which is significantly deeper than the total multilayer thickness (up to 300 nm) in both cases. This means that the ion beam interacts with a multilayer only by energy transfer, and not by changing the multilayer composition. Also, other effects such as elastic collisions with nuclei in the target material (nuclear stopping power  $S_n$ ) that become dominant near the end of the ion range can be neglected for the investigated multilayer thicknesses. Below we investigate the properties of the as-deposited films after irradiation treatment but before they were thermally annealed.

GISAXS intensity distributions measured on the same multilayer type, irradiated with oxygen ions with the same fluence,  $D_2 = 1 \times 10^{15}$  ions/cm<sup>2</sup>, and irradiation angle,  $\varphi_{\text{irr}} = 60^\circ$ , but with different energies of the oxygen ion (3, 1, and 15 MeV) are shown in Figs. 1(a), 1(b), and 1(c), respectively. For comparison, a GISAXS map of the nonirradiated sample is displayed in Fig. 1(d). The insets show the corresponding TEM images. All GISAXS maps show strong Bragg sheets (indicated by dashed lines) with different inclination angles with respect to the vectors of the reciprocal space  $Q_y$  and  $Q_z$ . The sheets are the consequence of the strong correlation in the QD and/or interface roughness positions. As shown in our

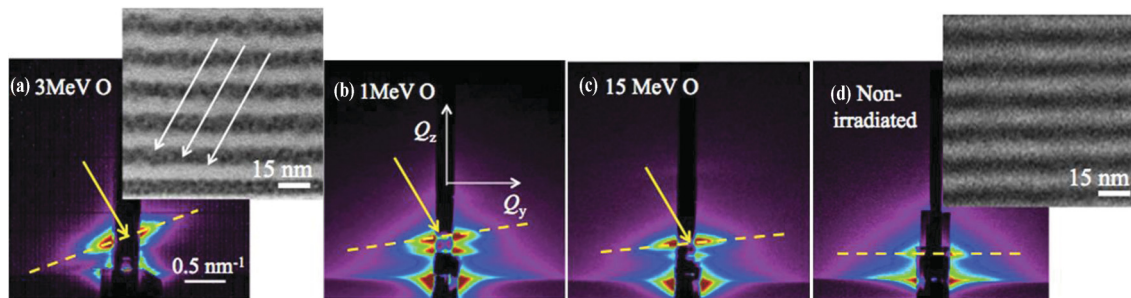


FIG. 1. (Color online) (a–c) GISAXS maps of (Ge + SiO<sub>2</sub>)/SiO<sub>2</sub> multilayer irradiated with  $1 \times 10^{15}$  ions/cm<sup>2</sup> oxygen ions with different energies under an angle of 60°, with respect to the multilayer surface. (d) GISAXS map of a nonirradiated sample. Dashed lines indicate Bragg sheets, while arrows indicate the irradiation direction. Insets: TEM images corresponding to the GISAXS image shown.

previous work,<sup>6</sup> ion-beam irradiation under specific conditions (3-MeV O ions; fluence,  $1 \times 10^{15}$  ions/cm<sup>2</sup>) causes formation and ordering of QDs and interface roughness features along the irradiation direction (indicated by the arrow). The tilt angle of the sheets for that specific case is perpendicular to the irradiation angle ( $\varphi_{\text{irr}}$ ). For the case of the nonirradiated multilayer, the sheets are parallel to the multilayer, i.e., they are along the  $Q_y$  axis. Therefore, the presence of the self-assembly caused by irradiation under some angle different from 90°, can be easily determined just by visual inspection of GISAXS maps. The values of the parameters describing the QD arrangement and their sizes can be obtained by fitting experimentally obtained maps using the model published in Ref. 6.

From Fig. 1 it follows that only 3-MeV ions cause the appearance of tilted Bragg sheets with the sheet angle approximately perpendicular to the irradiation direction. So, for that case, irradiation caused the formation and ordering of QDs along the irradiation direction. A detailed study of that system, i.e., of the QD size, distance, and arrangement type in the case of irradiation with 3-MeV O ions, is given in Ref. 8 for different irradiation angles, ion fluences, and multilayer types. The most important findings were summarized in a set of simple equations [Eqs. (1)–(3) in Ref. 8] that enables the estimation of nanoparticle sizes as well as the determination of their spacing and arrangement in the matrix.

Contrary to 3-MeV oxygen ions, Bragg sheets are just slightly tilted for the two other energies of the O beam, and they are more similar to the nonirradiated multilayer stack shown in Fig. 1(d). Slightly tilted sheets were observed earlier for very low irradiation fluencies<sup>8</sup> of 3-MeV O ions that produce small effects in the material resulting in very small agglomerates of Ge atoms (smaller than 1 nm) that are close together. As GISAXS is very sensitive to structural changes of Ge QDs in a SiO<sub>2</sub> matrix, we believe that 1- and 15-MeV ions do not cause significant structural changes in the material. A similar conclusion follows from the semicircular background intensity correlated with the size of the Ge clusters in Ge + SiO<sub>2</sub> layers. This means that ions with lower electronic stopping (1-MeV O ions,  $S_e \sim 1.4$  keV nm<sup>-1</sup>) do not cause significant diffusion and clustering of Ge atoms. The same is valid for 15-MeV O ions, although those ions have almost the same  $S_e$  as 3-MeV O. This indicates that, in addition to ion electronic stopping, another parameter plays an important role in the ordering of

Ge QDs. GISAXS maps showing the influence of 15-MeV O ions on multilayer type  $S_2$  for different irradiation angles are displayed in Figs. 2(a)–2(c). No significant changes with the irradiation angle are visible, especially if these results are compared with the effect produced by 3-MeV O ions.<sup>8</sup> So, the 15-MeV O ions have not produced changes in the material for any investigated irradiation angle. This result strongly indicates the importance of the ion velocity for QD formation and ordering. 15-MeV O ions are much faster during their passage through the multilayer, and the velocity effect<sup>13,14</sup> significantly reduces the ion beam’s ability to induce structural changes in the material.

We have also analyzed the influence of the thickness of the Ge-rich layer and the concentration of Ge atoms in it on the QD ordering. GISAXS maps showing the irradiation of different multilayer types with 1-MeV O ions under 60° are presented in Figs. 3(a)–3(c). For all multilayer types, differing by layer thickness and Ge content, the tilt angle of the Bragg sheets is nearly the same and practically equal to the nonirradiated case with sheets parallel to the  $Q_y$  axis. So, the effect of ordering was negligible for the different multilayer types after irradiation with 1-MeV O ions. From Figs. 2 and 3 it can be concluded that, regardless of the multilayer type or irradiation angle, tilted Bragg sheets perpendicular to the irradiation direction have not been observed for either 1- or 15-MeV O ions. The self-assembly of QDs was not efficient during irradiation at these two energies. From the numerical analysis of these maps we can conclude that the size of the clusters eventually formed by the irradiation process is smaller than 1 nm, and their separation within the layers is less than 1.5 nm. Ge atoms remain confined within the multilayer stack

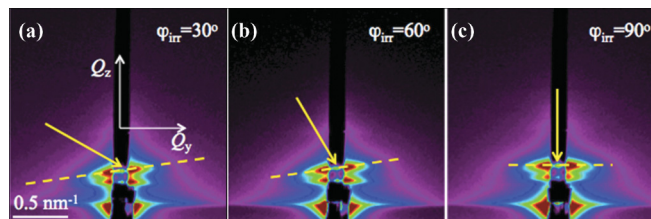


FIG. 2. (Color online) (a–c) GISAXS maps of (Ge + SiO<sub>2</sub>)/SiO<sub>2</sub> multilayers irradiated with  $1 \times 10^{15}$  ions/cm<sup>2</sup>, 15-MeV oxygen ions under different incident angles (indicated in the figure) with respect to the multilayer surface.

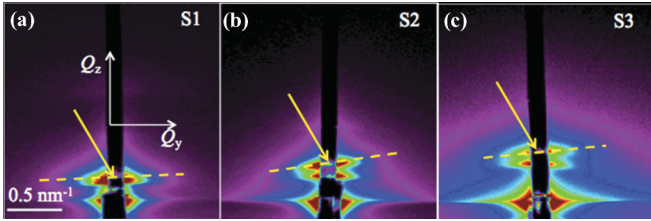


FIG. 3. (Color online) (a–c) GISAXS maps of different multilayer types ( $S_1$ – $S_3$ ) irradiated with  $1 \times 10^{15}$  ions/cm<sup>2</sup>, 1-MeV oxygen ions under  $60^\circ$  with respect to the multilayer surface.

prepared by the deposition whose parameters are given in Table I.

In addition, we have investigated the effect of irradiation with Si ions that have a significantly larger  $S_e$  value as reported in Table II. GISAXS maps for samples irradiated with 6- and 15-MeV Si ions are displayed in Fig. 4. The maps were measured perpendicular ( $\perp$ ) and parallel ( $\parallel$ ) to the ion irradiation plane.<sup>6,7</sup> Strongly tilted Bragg sheets and a strong semicircular intensity in the background are visible for the  $\perp$  configurations, showing the formation and regular ordering of QDs for both energies of Si ions used. In the maps measured in a  $\parallel$  configuration, lateral maxima are visible, showing the correlation of the QD positions within the Ge-rich layers. From GISAXS maps the mean separation of the Ge clusters formed can be calculated. For that purpose a specially developed paracrystal model, described in detail in Ref. 12, was applied. The obtained separations are  $L_1 = 5.5 \pm 0.1$  nm for 15-MeV Si and  $L_2 = 4.4 \pm 0.2$  nm for 6-MeV Si ions for the  $\parallel$  configuration. The mean values of the cluster sizes are found to be  $3.8 \pm 0.3$  nm for 15-MeV Si ions and  $3.0 \pm 0.4$  nm for 6-MeV Si ions. The distances for the  $\perp$  configuration were found to be elongated in comparison to the  $\parallel$  distances for the factors in  $(\sin \varphi_{\text{irr}})^{-1}$ , which is in agreement with our previous findings.<sup>8</sup> The separations between clusters obtained for different ion types were further used for the determination

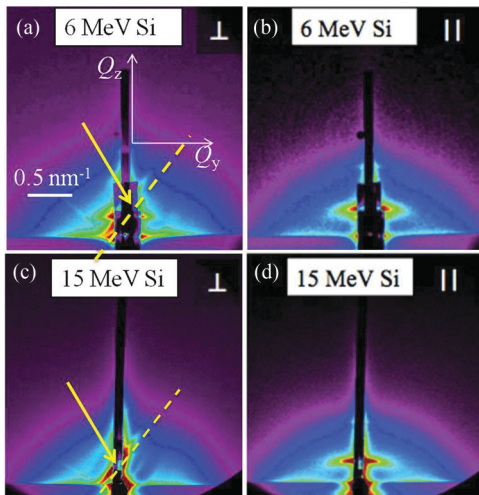


FIG. 4. (Color online) GISAXS maps of multilayers irradiated under  $60^\circ$  with (a, b) 6-MeV Si and (c, d) 15-MeV Si ions. The probing x-ray beam was perpendicular ( $\perp$ ) or parallel ( $\parallel$ ) to the irradiation plane as indicated in the upper right corner.

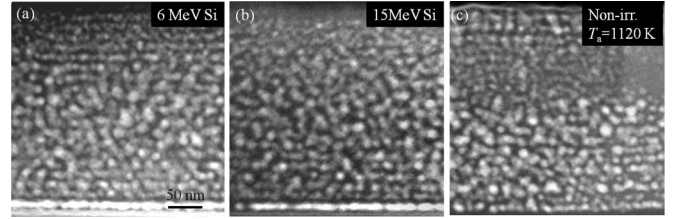


FIG. 5. STEM/HAADF (Z-contrast) images of films (a) irradiated with 6-MeV Si ions, (b) irradiated with 15-MeV Si ions, and (c) nonirradiated film annealed at 1120 K for a duration of 1 h.

of ion track radii in the investigated systems, as demonstrated in Sec. IV.

It is important to note that the after-irradiation annealing treatment (which was not used for the films presented here) causes an increase in the mean separation between clusters. For example, if annealing at  $T = 1073$  K is applied after the irradiation,<sup>8</sup> the mean separation of the clusters formed increases due to the Ostwald ripening process,<sup>15</sup> which causes degradation of smaller clusters. Therefore, the separations of Ge clusters formed by Si ion irradiation are smaller than the separations of Ge clusters formed by O-ion irradiation followed by annealing at 1073 K.<sup>8</sup>

Si ions, 6 and 15 MeV, strongly influence the multilayer structure and cause very prominent QD formation as shown by the TEM images of the irradiated films in Figs. 5(a) and 5(b). In these figures, a very strong clustering process is shown for both irradiated films, especially when the figures are compared to the TEM image of the film irradiated with 3-MeV O ions [Fig. 1(a)]. Traces of multilayer destruction and intermixing of neighboring layers are also visible. The destruction is less prominent for the 6-MeV-irradiated film, where the lower and upper layers are preserved after irradiation. The film irradiated with 15-MeV Si ions retained the layered structure only in the few layers that are close to the substrate. A similar destruction effect is produced when a standard 1-h annealing at 1120 K is applied [Fig. 5(c)]. After the annealing process, the lower and upper layers are also preserved, as for the 6-MeV Si irradiation. This strongly implies that the temperature caused by ion passage through the Ge-rich layer was close to 1120 K for the 6-MeV Si ions and above this for the 15-MeV Si ions. Also, shrinkage of the neighboring layers associated with ion-beam compaction or plastic flow can be seen.<sup>11</sup>

#### IV. THERMAL SPIKE MODEL: CALCULATION OF SYSTEM PARAMETERS

In this section we calculate the parameters of the investigated systems needed to determine the temperature profiles inside the ion tracks. The temperature profiles are used to explain the experimentally observed structural properties of the irradiated films. For that purpose we apply the analytical thermal spike model and method for calculation of the ion track radii.<sup>8,13</sup>

According to the thermal spike model, the temperature increase  $\Delta T(\mathbf{r}, t)$  caused by ion-beam passage is

given by

$$\Delta T(\mathbf{r}, t) = Q(t) \exp \left[ - \frac{(x - x_0 - (z - z_0) / \tan(\varphi_{\text{irr}}))^2}{w_x(t)^2} - \frac{(y - y_0)^2}{w_y(t)^2} \right], \quad (1)$$

where  $\mathbf{r} = (x, y, z)$  is the position coordinate;  $\mathbf{r}_0 = (x_0, y_0, z_0)$  denotes the center of the ion track;  $t$  is the time; the three time-dependent functions,

$$w_x(t) = \begin{cases} \frac{w_0 t_0^{1/2}}{\sin(\varphi_{\text{irr}})}, & t \leq t_0, \\ \frac{w_0 t^{1/2}}{\sin(\varphi_{\text{irr}})}, & t > t_0, \end{cases} \quad w_y(t) = \begin{cases} w_0 t_0^{1/2}, & t \leq t_0, \\ w_0 t^{1/2}, & t > t_0, \end{cases}$$

$$Q(t) = \begin{cases} T_{\text{max}} \frac{t}{t_0}, & t \leq t_0, \\ T_{\text{max}} \frac{t_0}{t}, & t > t_0, \end{cases} \quad (2)$$

describe the propagation of heat within the material, where  $T_{\text{max}}$  is the peak temperature in the center of the ion track;  $t_0$  is the time when the temperature inside the ion track is the highest; and  $w_0$  is a parameter determined by the material properties. The irradiation direction is placed in the  $x$ - $z$  plane. The value  $a_0 = w_0 t_0^{1/2}$  is the characteristic width of the initial temperature profile at time  $t_0$ .

The peak of the temperature increase  $T_{\text{max}}$  is given by<sup>13</sup>

$$T_{\text{max}} = S_e g / (\pi \rho c w_0^2 t_0), \quad (3)$$

where  $g$  is the fraction of the deposited energy  $S_e$  transferred into the energy of the thermal spike,  $S_e$  is the electronic stopping of the ion in the material,  $\rho$  is the material density, and  $c$  is its specific heat capacity. The temperature achieved in the system caused by ion passage is

$$T(\mathbf{r}, t) = T_{\text{IRR}} + \Delta T(\mathbf{r}, t), \quad (4)$$

where  $T_{\text{IRR}}$  is the temperature at which the irradiation is performed. The parameters that are needed for calculation of the temperature profiles in the investigated systems are the following:  $S_e$ ,  $a_0$ ,  $\rho$ ,  $g$ ,  $c$ ,  $t_0$ , and  $T_{\text{IRR}}$ . Their values for the investigated systems are given in the following. The value of electronic stopping  $S_e$  in the material can be easily determined by the SRIM code.<sup>16</sup> For a realistic determination of  $S_e$ , the atomic composition and density of the system should be known. We have determined the densities of our systems using a combination of RBS (which gives us the atomic percentages of the constituent elements per unit area) with GISAXS and TEM (which provide us the thickness of the layers). Due to the multilayer structure of the films, with different Ge percentages in the Ge-rich layers, we have calculated the parameters for two types of materials: (i) a Ge + SiO<sub>2</sub> mixture with 12.7% Ge atoms and (ii) a Ge + SiO<sub>2</sub> mixture with 23.5% Ge atoms. The determined density values are listed in Table II. The constant  $g$  has the value of 0.4 for low ion velocities, but  $g = 0.2$  for high ion velocities.<sup>13</sup>

Determination of the initial temperature width parameter  $a_0$  was performed using the procedure described in Ref. 9. Namely, we use the distances between Ge clusters ( $L_1$  and  $L_2$ ) formed in the same multilayer type by using 6- and 15-MeV Si ions. The mean value for distances between clusters can be

related to  $a_0$  using the following equation:<sup>9</sup>

$$a_0^2 = \frac{L_2^2 - L_1^2}{4 \ln(S_{e2}/S_{e1})}, \quad (5)$$

where  $L_1$  and  $L_2$  are the measured mean values for distances between the clusters formed by 6 and 15 MeV, respectively, obtained from the analysis of GISAXS maps. Using the values of  $L_1$  and  $L_2$  and applying Eq. (5),  $a_0 = 3.5 \pm 0.6$  nm was calculated. The value of  $a_0$  can be determined only for films irradiated with Si ions, as this method requires the formation of clusters by irradiation only. Due to the same preparation of all films and similar percentages of Ge atoms, we can assume that the  $a_0$  value is similar for all studied films. This assumption is supported by the value of  $a_0$  found for the (Ni + SiO<sub>2</sub>)/SiO<sub>2</sub> system, which is practically the same as the value obtained here.<sup>9</sup> This value is smaller than the  $a_0 = 4.5$  nm found earlier for insulators<sup>13</sup> but higher than the value needed to describe ion tracks in vitreous silica.<sup>17</sup> Possibly, the introduction of a semiconductor in SiO<sub>2</sub> results in an increase in  $a_0$ .<sup>18</sup>

Another task is the determination of the material specific heat capacity without direct measurements. The material is deposited at RT, and its density and stoichiometry are different from those of standard fused silica, so we cannot apply the heat capacity values of standard SiO<sub>2</sub>. Therefore, we have used the Dulong-Petit law and treated our material as a mixture of Si, O, and Ge atoms at the ratio found from RBS measurements. Using these assumptions, we obtained the calculated values for specific heat capacities listed in Table II. The obtained values correspond to the upper limit of the heat capacity for the materials in question. The value of  $t_0$  is in the range of picoseconds<sup>19</sup>—we take  $t_0 = 1$  ps—but as explained in Ref. 9, the maximal temperature and width of ion tracks are not dependent on this quantity for the high-temperature regime.

Thus, we have determined all parameters needed to estimate the temperature increase in the material caused by ion irradiation. All temperature parameters characteristic for the investigated systems were calculated using these values and Eqs. (1)–(3). For each material, two characteristic temperatures were calculated: the maximal temperature in the system  $T_{\text{max}}$  and the temperature achieved at  $r = a_0$  [denoted  $T(r = a_0)$ ]. The maximal temperature is achieved at time  $t = t_0$ , and it decreases rapidly with time according to Eq. (1). The time dependence of the thermal spike in the film is shown in Fig. 6. This figure shows that the maximum temperature of the thermal spike decreases with time and it is 50% lower after a duration of  $2t_0$ . So, the time during which the temperatures are close to  $T_{\text{max}}$  is very short, and also, the maximal radius of the ion track  $r(T \sim T_{\text{max}})$  is very small at these temperatures. Therefore, we consider the temperature  $T(r = a_0)$  to be an important temperature for the estimation of the influence of ion passage on changes in the materials. All calculated parameters are listed in Table II. A similar requirement was found for other temporal-sensitive processes like growth of nanohillocks at ion impact sites.<sup>20,21</sup>

## V. DISCUSSION

Here we discuss the experimentally measured structural properties of films irradiated with various ion types. For

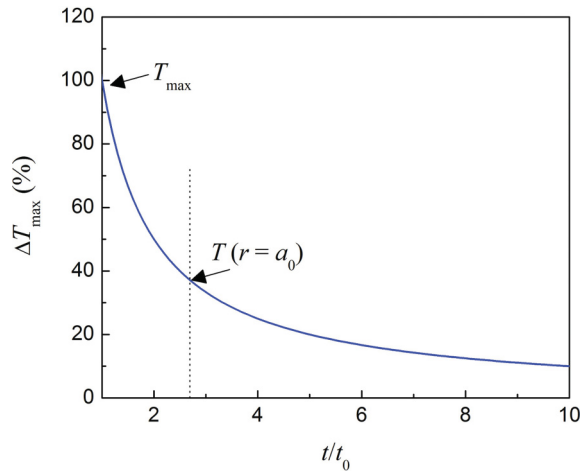


FIG. 6. (Color online) Dependence of the maximal temperature increase ( $\Delta T_{\max}$ ) in the film on time. The maximal temperature in the system ( $T_{\max}$ ) achieved in time  $t = t_0$  and the characteristic temperature achieved for width  $r = a_0$  and  $t = t_0$  are indicated by arrows.

the explanation we use the temperature-increase parameters determined in the previous section. We compare the structural changes in films caused by irradiation with the changes that are a consequence of standard thermal annealing. Although this comparison cannot be direct due to the fact that the temperature pulse caused by ion passage is very short (in the range of picoseconds) compared to that caused by standard annealing, some conclusions can be drawn.

According to our previous work on similar or the same systems, four characteristic temperatures can be recognized for the (Ge + SiO<sub>2</sub>)/SiO<sub>2</sub> multilayer system.<sup>22–24</sup> First is the temperature at which weak clustering of Ge atoms starts. A change in the material and a weak redistribution of deposited Ge atoms start already at  $570 \pm 50$  K during the postdeposition annealing process when the deposition is performed at RT.<sup>22</sup> The formation of small Ge clusters is found at a slightly lower temperature (about 520 K) when it occurs during deposition.<sup>24</sup> The difference can be attributed to the diffusion constant, which is larger at the growing surface (and causes clustering during growth) than for the bulk (clustering during afterdeposition annealing). The clusters formed are fully amorphous and usually not regular in shape.<sup>22,23</sup> Second is the temperature of the prominent Ge clustering and beginning of the Ge crystallization process. Prominent Ge clustering starts at  $820 \pm 50$  K.<sup>22</sup> The crystallization of Ge atoms also starts at approximately the same temperature. However, the clusters formed are not fully crystalline; instead, mixed (crystalline + amorphous) Ge clusters are formed.<sup>23</sup> The third important temperature is that of the strong clustering and crystallization process. Significant and relatively fast changes in the material occur at  $1020 \pm 30$  K. The clusters formed at this temperature are fully crystalline and approximately spherical in shape.<sup>22,23</sup> And finally, the temperature at which destruction of the multilayer film structure and Ge loss from the film start is  $1120 \pm 30$  K as shown in Fig. 5(c) here as well as in Refs. 22 and 23. So we expect that the changes caused by ions will be smaller than or equal to the changes caused by long-time annealing or deposition at elevated temperatures, due to the

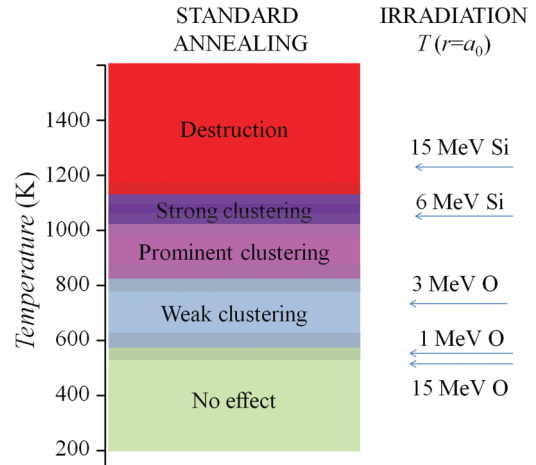


FIG. 7. (Color online) Comparison of the temperature regimes for standard thermal annealing versus ion-beam irradiation concerning effects induced in the material. Shaded areas represent uncertainties for determination of characteristic temperatures.

short duration of the temperature pulses. A scheme showing a comparison of the temperature-induced effects of standard annealing versus irradiation is shown in Fig. 7.

First, we focus on the system irradiated with 3-MeV O ions, for which the GISAXS data are shown in Fig. 1(a). The maximal temperature and the temperature at  $r = a_0$  for that system (Ge-rich layer with 12.7% Ge) are 1457 and 735 K. The estimated temperatures for  $r = a_0$  are in excellent agreement with the observed structural changes and the characteristic temperatures that are found to be important for Ge clustering using a standard annealing treatment (shown in Fig. 7). The maximal temperature is not significantly higher than the destruction temperature. So the 3-MeV O ions are found to be optimal for the production of ordered Ge clusters in the investigated system.

The second system is a multilayer irradiated with 1-MeV O ions. The temperature of  $T(r = a_0) = 556$  K is estimated for a Ge-rich layer (12.7% Ge) for the given ion type and material. These temperatures are below the temperatures that are found to be important for clustering of Ge atoms using standard annealing or deposition at elevated temperatures. Therefore the absence of changes in the material observed by GISAXS [Fig. 1(b)] is in agreement with the findings of the temperature-increase analysis.

The third system [Fig. 1(c)], a multilayer irradiated with 15-MeV O ions, also does not show any significant structural changes after irradiation, though the electron stopping of 15-MeV O ions is almost identical to the stopping of 3-MeV O ions. This observation can be explained by the velocity effect. Due to the high velocity, the energy transfer is less effective so the temperature increase is smaller. We have used a value of the constant  $g = 0.2$  instead of the 0.4 that is used for the description of the other systems. The calculated temperatures for this system are even lower than those found for 1-MeV O ions. So the absence of structural changes is in excellent agreement with the temperature estimation.

A similar temperature behavior is found for the system with a slightly higher Ge content. The temperature changes in the system with 23.5% Ge are very similar to those for the system

with 12.7% Ge (Table II). Therefore, we conclude that small differences in Ge content do not cause significant differences in the temperature changes or, consequently, in the structural properties of the irradiated Ge-based multilayer. The same is found experimentally; the data are shown in Fig. 3.

Finally, we focus on the effects of Si ions. As reported in Table II, the temperatures caused by Si ions are considerably higher than those produced by O ions. The peak temperatures are higher than the melting temperature of fused quartz (about 2000 K) for both Si-ion energies and all multilayer types.<sup>17,25</sup> The temperatures estimated for  $r = a_0$  (1040 and 1224 K for 6- and 15-MeV Si ions respectively) are below the melting temperature of fused silica. However, they are close to the limiting temperature for the multilayer destruction (1120 K) that is caused by standard thermal annealing. The changes caused by Si-ion passage are significant, and the observed structural changes are in good agreement with the temperature estimations. Precisely, large and clearly separated clusters are formed, according to the TEM images in Fig. 5, but there is no loss of Ge in these films. The multilayer structure is not completely destroyed but disintegration has started to occur. The destruction is more pronounced for the film irradiated with 15 MeV than for 6-MeV Si ions, in accordance with the higher temperature estimated for  $r = a_0$ . So, we conclude that the structural changes in the (Ge + SiO<sub>2</sub>)/SiO<sub>2</sub> multilayer system can be well described and predicted by the temperature increase  $T(r = a_0, t = t_0)$ .

## VI. CONCLUSIONS

The influence of different ion-beam properties on the self-assembly process in (Ge + SiO<sub>2</sub>)/SiO<sub>2</sub> multilayers was studied. It was shown that self-ordering can be explained by two important ion properties: ion electronic stopping and

the efficiency of deposited energy transfer to the thermal spike. The ordering can be easily determined by visual inspection of GISAXS maps through tilted Bragg sheets that are perpendicular to the ion irradiation direction if ordering along the irradiation direction occurred. The temperature increase in the system caused by ion-beam passage was estimated using the thermal spike model and cluster separation distribution. Structural changes in the films caused by ion beams were compared with those obtained by standard thermal annealing. Our results show a good correlation between the estimated temperatures and the observed structural changes in the investigated systems.

The most effective formation and ordering of Ge QDs were achieved using a 3-MeV O beam. On the contrary, 15-MeV O ions with the same value of  $S_e$  but with a lower value for the energy efficiency transfer  $g$  did not cause self-assembly. Using Si ions, mixing and destruction of multilayers occurred due to the high-temperature increase induced by ion beams. The temperature at which destruction of the multilayer film structure and Ge loss start was found to be around 1100 K in the case of thermal annealing, which corresponds to the temperature increase caused by irradiation of the film with 15-MeV Si ions.

## ACKNOWLEDGMENTS

The authors are grateful to Medeja Gec for preparation of samples for TEM measurements and to Aleksa Pavlešin for assistance during sample preparation. I.B.R., M.B., M.K., I.B., M.J., and N.R. acknowledge support from the Croatian Ministry of Science Higher Education and Sport; V.H. acknowledges support from the Czech Science Foundation (Project No. P204-11-0785); and G.D. acknowledges support from the Slovenian Research Agency (Grant No. P2-0084).

\*Correspondence author: iva@irb.hr

<sup>1</sup>R. Hanson, *Rev. Mod. Phys.* **79**, 1217 (2009).

<sup>2</sup>A. Konchenko, Y. Nakayama, I. Matsuda, S. Hasegawa, Y. Nakamura, and M. Ichikawa, *Phys. Rev. B* **73**, 113311 (2006).

<sup>3</sup>A. Dowd, R. G. Elliman, M. Samoc, and B. Luther-Davies, *Appl. Phys. Lett.* **74**, 239 (1999).

<sup>4</sup>J. K. Shen, X. L. Wu, C. Tan, R. K. Yan, and X. M. Bao, *Phys. Lett. A* **300**, 307 (2002).

<sup>5</sup>S. K. Ray and K. Das, *Opt. Mater.* **27**, 948 (2005).

<sup>6</sup>M. Buljan, I. Bogdanović-Radović, M. Karlušić, U. V. Desnica, G. Dražić, N. Radić, P. Dubček, K. Salamon, S. Bernstorff, and V. Holy, *Appl. Phys. Lett.* **95**, 063104 (2009).

<sup>7</sup>M. Buljan, I. Bogdanović-Radović, M. Karlušić, U. V. Desnica, N. Radić, N. Skukan, G. Dražić, M. Ivanda, O. Gamulin, Z. Matej, V. Valeš, J. Grenzer, T. W. Cornelius, H. T. Metzger, and V. Holy, *Phys. Rev. B* **81**, 085321 (2010).

<sup>8</sup>M. Buljan, I. Bogdanović-Radović, M. Karlušić, U. V. Desnica, N. Radić, M. Jakšić, K. Salamon, G. Dražić, S. Bernstorff, and V. Holy, *Phys. Rev. B* **84**, 155312 (2011).

<sup>9</sup>M. Buljan, M. Karlušić, I. Bogdanović-Radović, M. Jakšić, S. Bernstorff, K. Salamon, and N. Radić, *Appl. Phys. Lett.* **101**, 103112 (2012).

<sup>10</sup>The double sheets seen in GISAXS maps are the consequence of the existence of two sample parts (irradiated and nonirradiated), having different thicknesses. Both parts are illuminated simultaneously by an x-ray beam during GISAXS measurements. The first is the nonirradiated multilayer. Only a very small portion of that part is illuminated, so the signal comes mostly from the second, irradiated part. The thickness change is caused by ion-beam-induced compaction or plastic flow (see Ref. 11), which induces shrinkage of the multilayer. Since the irradiated area is smaller than the spot size of the photon beam, both contributions in GISAXS maps can be seen.

<sup>11</sup>A. Benyagoub, S. Klaumunzer, and M. Toulemonde, *Nucl. Instrum. Methods B* **146**, 449 (1998).

<sup>12</sup>M. Buljan, N. Radić, S. Bernstorff, G. Dražić, I. Bogdanović-Radović, and V. Holy, *Acta Crystallogr. Sec. A* **86**, 124 (2012).

<sup>13</sup>G. Szenes, *Phys. Rev. B* **51**, 8026 (1995).

<sup>14</sup>G. Szenes, *Nucl. Instrum. Methods B* **269**, 174 (2011).

<sup>15</sup>K. H. Heining, T. Muller, B. Schmidt, M. Strobel, and W. Moeller, *Appl. Phys. A* **77**, 17 (2003).

<sup>16</sup>J. J. F. Ziegler, *Nucl. Instrum. Methods B* **219**, 1027 (2004).

- <sup>17</sup>M. Toulemonde, W. J. Weber, G. Li, V. Shutthanandan, P. Kluth, T. Yang, Y. Wang, and Y. Zhang, *Phys. Rev. B* **83**, 054106 (2011).
- <sup>18</sup>G. Szenes, *Nucl. Instrum. Methods B* **280**, 88 (2012).
- <sup>19</sup>O. Osmani, N. Medvedev, M. Schleberger, and B. Rethfeld, *Phys. Rev. B* **84**, 214105 (2011).
- <sup>20</sup>G. Szenes, F. Paszti, A. Peter, and D. Fink, *Nucl. Instrum. Methods B* **191**, 186 (2002).
- <sup>21</sup>M. Karlušić and M. Jakšić, *Nucl. Instrum. Methods B* **280**, 103 (2012).
- <sup>22</sup>K. Salamon, O. Milat, M. Buljan, U. V. Desnica, N. Radić, P. Dubček, and S. Bernstorff, *Thin Solid Films* **517**, 1899 (2009).
- <sup>23</sup>M. Buljan, U. V. Desnica, M. Ivanda, N. Radić, P. Dubček, G. Dražić, K. Salamon, S. Bernstorff, and V. Holy, *Phys. Rev. B* **79**, 035310 (2009).
- <sup>24</sup>S. R. C. Pinto, A. G. Rolo, M. Buljan, A. Chahboun, S. Bernstorff, N. P. Barradas, E. Alves, R. J. Kashtiban, U. Bangert, and M. J. M. Gomes, *Nanoscale Res. Lett.* **6**, 341 (2011).
- <sup>25</sup>G. Szenes, *Appl. Phys. Lett.* **81**, 4622 (2002).